

Anisotropic surface waves under a vertical electromagnetic force. Part 2. Experimental demonstration

By I. S. ROBINSON

Institute of Oceanographic Sciences, Bidston Observatory,
Birkenhead, Cheshire

(Received 2 April 1974)

It was shown theoretically in part 1 (Shercliff 1969) that, when a horizontal magnetic field and electric current field are imposed upon a conducting liquid with a free surface, waves excited at the surface have an anisotropic dispersion relation. Here the possibility of demonstrating this phenomenon in the laboratory is considered. The analysis is completed for waves at the interface between a conducting and non-conducting fluid of similar density, taking full account of surface tension, and then viscosity. Surface tension is found to have a considerable influence in reducing the degree of anisotropy to be expected. The problem of choosing suitable experimental parameters is discussed, and an apparatus is described in which it was possible to demonstrate the existence of anisotropic surface waves, and to compare the phase velocity with the theoretical results. Also, an experiment is described which verifies the relationship between the orientation of the anisotropy and the relative orientation of the imposed magnetic and current fields.

1. Introduction

Part 1 (Shercliff 1969) showed theoretically that waves on the surface of a conducting liquid, in the presence of a vertical electromagnetic body force due to imposed horizontal magnetic and electric current fields, propagate anisotropically. This can be attributed directly to the boundary condition on the current density \mathbf{j} , which can have no component normal to the fluid surface, at the surface. Consequently, the current component normal to wave troughs and crests has associated with it a $\mathbf{j} \times \mathbf{B}$ force (\mathbf{B} being the constant, uniform, horizontal magnetic flux density), which must always be normal to the surface, and cannot influence wave propagation. The current component parallel to wave crests, however, is always horizontal, and its associated $\mathbf{j} \times \mathbf{B}$ force is always vertical, acting to help or hinder the gravity force, and consequently affecting surface wave propagation. The phase and group velocity of plane surface waves are therefore dependent upon the orientation of the wave normal relative to the imposed current density vector in the undisturbed state (i.e. the waves propagate anisotropically).

In this paper, the experimental possibilities of this phenomenon are explored, and some laboratory experiments are described, the results of which demonstrate

the existence of MHD anisotropic surface waves, and substantiate the basic theoretical work of Shercliff. One of the motivations behind a laboratory demonstration is the fact that, unlike most other anisotropic wave systems encountered in physics, surface waves on a fluid can be easily and directly observed, and could possibly be used as an aid to teaching the theory of anisotropic waves.

In presenting typical plots of the dispersion relation, Shercliff chooses to ignore the effect of surface tension and viscosity, in order to simplify the problem. He also makes suggestions as to the choice of suitable experimental parameters to be used in any laboratory demonstration of the phenomenon, and shows that with mercury as a working fluid the surface tension α may be considered to be of negligible effect for a given set of reasonable parameters. While such an assumption may be justified in the ordinary hydrodynamic (OHD) case, it is not necessarily so for the MHD case, since, with an upward acting $\mathbf{j} \times \mathbf{B}$ force, the tendency is to increase the wavenumber k of surface waves of a given frequency, in one direction, thus increasing the magnitude of $\alpha k^2/\rho g$, which determines the influence of surface tension. Now surface tension has the effect of decreasing the wavenumber for a given frequency, and consequently counteracts the influence of the upward $\mathbf{j} \times \mathbf{B}$ force, thus reducing the degree of anisotropy from that which would be expected with zero surface tension. By similar reasoning, the influence of viscosity can be negligible for a given frequency of OHD waves, but may be significant in the anisotropic MHD case. The need for a complete analysis is further reinforced when considering the waves that occur at the interface between a conducting and non-conducting fluid closely matched in density. Such a system, in reducing the effective gravity force on the waves, enables the $\mathbf{j} \times \mathbf{B}$ force to compete with it more easily, but at the same time increases the relative influence of surface tension and viscosity.

Hence, while it is instructive to ignore surface tension and viscosity in the first instance, to clarify the theoretical analysis, it is necessary to consider their influence in detail when designing an experimental demonstration of the waves.

The only other experimental work in the literature related to this investigation is Baker (1965) and Duc (1968), on the MHD Rayleigh–Taylor instability. Since the stability equation for the Rayleigh–Taylor instability is essentially the same as the dispersion relation for surface waves, the experimental evidence of strongly anisotropic instabilities forms a basis for confidence in the theory of anisotropy in surface waves.

2. Theoretical dispersion relation

We shall make the same basic assumptions as Shercliff. (i) The magnetic field associated with the imposed electric current is negligible compared with the imposed magnetic field. (It follows that induced e.m.f. due to $\mathbf{E} = -\partial\mathbf{B}/\partial t$ may be ignored.) (ii) The perturbation of the imposed current by induced e.m.f. is negligible. (Thus ohmic damping is ignored.) (iii) Small-amplitude waves will be considered (i.e. the perturbation equations of motion are linearizable). (iv) The analysis is for plane waves with parallel troughs and crests, although any linearizable waves could be Fourier analysed into these.

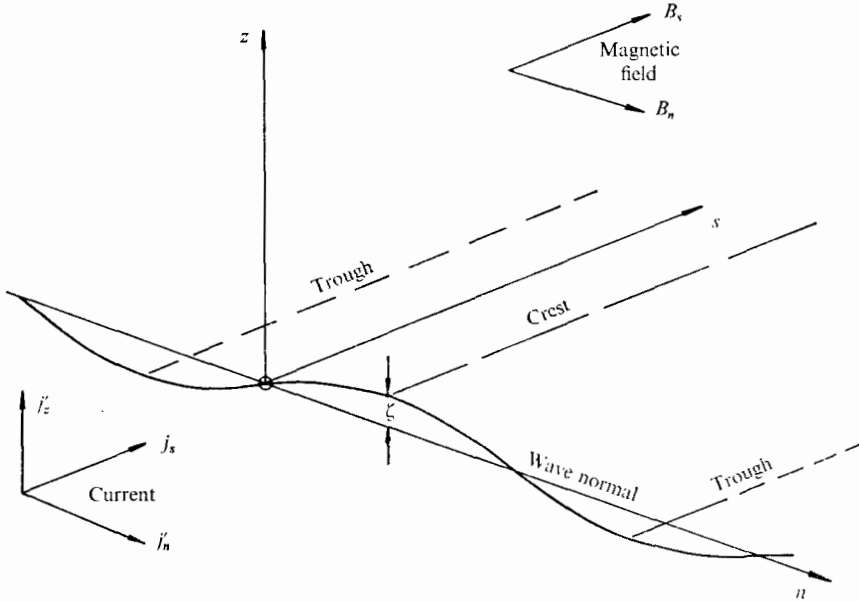


FIGURE 1

Let the upper, non-conducting fluid be denoted by subscript 1 and the lower, conducting fluid by 2. Consider the co-ordinate system of figure 1, with s a horizontal direction parallel to the wave crests, and n normal to them.

2.1. *Inviscid case*

If we consider only the motion in the z, n plane (i.e. that associated with the plane waves), then

$$\nabla^2 \phi_1 = 0, \tag{1}$$

where ϕ is a two-dimensional velocity potential; and, following Shercliff's argument, $\nabla \times (\mathbf{j} \times \mathbf{B})$ has no s component, so that

$$\nabla^2 \phi_2 = 0. \tag{2}$$

The two-dimensional equations of motion for the upper and lower fluids, respectively, are

$$\nabla(\rho_1 \partial \phi_1 / \partial t + p_1 + \rho_1 g z) = 0, \tag{3}$$

$$\nabla(\rho_2 \partial \phi_2 / \partial t + p_2 + [\rho_2 g + j_s B_n] z) = \mathbf{j}' \times \mathbf{B}_s, \tag{4}$$

where $\mathbf{j} \times \mathbf{B}$ in the z, n plane is expressed as $-j_s B_n \mathbf{i} + \mathbf{j}' \times \mathbf{B}_s$, \mathbf{j}' being the current component in the z, n plane. (We ignore the $\mathbf{j}' \times \mathbf{B}_n$ term, which is in the s direction, and does not contribute to the wave motion.) Now, since $\mathbf{j}' \times \mathbf{B}_s$ is always

normal to the interface $z_0 = \zeta \exp \{i(\omega t - kn)\}$, integrating (3) and (4) along the interface, assuming periodic motion, results in

$$\rho_1 \frac{\partial \phi_1}{\partial t} + p_1 + \rho_1 g z_0 = 0 \quad \text{at } z = z_0 \quad (5)$$

and
$$\rho_2 \frac{\partial \phi_2}{\partial t} + p_2 + (\rho_2 g + j_s B_n) z_0 = 0 \quad \text{at } z = z_0. \quad (6)$$

Now the interfacial condition on pressure is

$$p_2 = p_1 - \alpha \frac{\partial^2 z_0}{\partial n^2},$$

and substituting this in (5) and (6) gives

$$\rho_2 \left(\frac{\partial \phi_2}{\partial t} \right)_{z=z_0} + (\rho_2 g + j_s B_n) z_0 = \rho_1 \left(\frac{\partial \phi_1}{\partial t} \right)_{z=z_0} + \rho_1 g z_0 + \alpha \frac{\partial^2 z_0}{\partial n^2}. \quad (7)$$

The linearized kinematic interfacial condition is

$$\left(\frac{\partial \phi_1}{\partial z} \right)_{z=z_0} = \left(\frac{\partial \phi_2}{\partial z} \right)_{z=z_0} = \frac{\partial z_0}{\partial t} = i\omega z_0; \quad (8)$$

and the other boundary condition required is that, at the top and bottom of the fluid space, the normal velocity is zero (the upper fluid has a lid), i.e.

$$\partial \phi_1 / \partial z = 0 \quad \text{at } z = +h_1, \quad \partial \phi_2 / \partial z = 0 \quad \text{at } z = -h_2, \quad (9)$$

where h_1, h_2 are the respective depths of the upper and lower fluids. Using (8) and (9), (1) and (2) may be solved to yield

$$\phi_1 = (i\omega/k) z_0 \{ \sinh kz - \coth kh_1 \cosh kz \}, \quad (10a)$$

$$\phi_2 = (i\omega/k) z_0 \{ \sinh kz + \coth kh_2 \cosh kz \}. \quad (10b)$$

For (10) to be compatible with the pressure condition (7), the constraint required is the dispersion relation $\omega = f(k)$, obtained by substituting (10) in (7), and making the small-amplitude wave approximation that

$$(\partial \phi / \partial t)_{z=z_0} = (\partial \phi / \partial t)_{z=0}.$$

Hence
$$(\rho_1 \coth kh_1 + \rho_2 \coth kh_2) \omega^2 = k \{ (\rho_2 - \rho_1) g + j_s B_n + \alpha k^2 \}. \quad (11)$$

This is the inviscid dispersion relation for two-fluid interfacial waves, allowing for surface tension.

2.2. Viscous case

Again we consider plane waves, and hence only the motion in the z, n plane. The equations of motion are

$$\frac{\partial u}{\partial t} + \frac{1}{\rho_2} \nabla p_2 = - \left(g + \frac{j_s B_n}{\rho_2} \right) \mathbf{i} + \frac{\mathbf{j}' \times \mathbf{B}_s}{\rho_2} + \nu_2 \nabla^2 \mathbf{u}, \quad (12)$$

$$\frac{\partial u}{\partial t} + \frac{1}{\rho_1} \nabla p_1 = -g \mathbf{i} + \nu_1 \nabla^2 \mathbf{u}. \quad (13)$$

Also, in both fluids
$$\nabla \cdot \mathbf{u} = 0. \quad (14)$$

We again split $\mathbf{j} \times \mathbf{B}$ in the z, n plane into two parts,

$$\mathbf{j}' \times \mathbf{B}_s - j_s B_n \mathbf{i}.$$

Following Lamb (1932, art. 349), we let

$$u_n = -\frac{\partial \phi}{\partial n} - \frac{\partial \psi}{\partial z}, \quad u_z = -\frac{\partial \phi}{\partial z} + \frac{\partial \psi}{\partial n}. \tag{15}$$

Equation (14) is satisfied if $\nabla^2 \phi = 0;$ (16)

and (12) and (13) are satisfied if $\partial \psi / \partial t = \nu \nabla^2 \psi,$ (17)

provided that $\nabla \times (\mathbf{j} \times \mathbf{B})$ has no component in the s direction. Substituting (17) in (12) and (13), and using (16) gives

$$\nabla \left(\frac{p_2}{\rho_2} - \frac{\partial \phi_2}{\partial t} + \left[g + \frac{j_s B_n}{\rho_2} \right] z \right) = \frac{\mathbf{j}' \times \mathbf{B}_s}{\rho_2}$$

and

$$\nabla \left(\frac{p_1}{\rho_1} - \frac{\partial \phi_1}{\partial t} + gz \right) = 0.$$

Integrating these along the interface $z = z_0 = \zeta \exp(ikn + \sigma t)$ with $\mathbf{j}' \times \mathbf{B}_s$ always normal to the interface gives

$$\left. \begin{aligned} p_2 &= \rho_2 \frac{\partial \phi_2}{\partial t} - (\rho_2 g + j_s B_n) z \\ p_1 &= \rho_1 \frac{\partial \phi_1}{\partial t} - \rho_1 g z \end{aligned} \right\} \text{ at } z = z_0. \tag{18}$$

Now we take

$$\left. \begin{aligned} \phi_1 &= (A_1 \exp -kz + B_1 \exp kz) \exp(ikn + \sigma t), \\ \psi_1 &= (C_1 \exp -m_1 z + D_1 \exp m_1 z) \exp(ikn + \sigma t), \\ \phi_2 &= (A_2 \exp kz + B_2 \exp -kz) \exp(ikn + \sigma t), \\ \psi_2 &= (C_2 \exp m_2 z + D_2 \exp -m_2 z) \exp(ikn + \sigma t), \end{aligned} \right\} \begin{array}{l} z > 0, \\ z < 0, \end{array} \tag{19}$$

which satisfy (16) and (17), provided

$$m^2 = k^2 + \sigma/\nu. \tag{20}$$

For simplicity, we assume infinite height of the top fluid and infinite depth of the bottom fluid, so that one boundary condition is for finite motion as $z \rightarrow \pm \infty$. Hence, $B_1 = B_2 = 0$, and, provided m has its real part positive, $D_1 = D_2 = 0$.

The other boundary conditions are on the normal velocities at the interface, i.e. to first order

$$u_{z1} = u_{z2} = \partial \zeta / \partial t \quad \text{at } z = 0, \tag{21}$$

and the stress conditions at the interface

$$P_{zz2} - P_{zz1} = \alpha \partial^2 \zeta / \partial n^2 \tag{22}$$

and $P_{nz2} = P_{nz1},$ (23)

where $P_{zz} = -p + 2\mu \frac{\partial u_z}{\partial z}$ and $P_{nz} = \mu \left(\frac{\partial u_z}{\partial n} + \frac{\partial u_n}{\partial z} \right),$ (24)

Substituting (19) in (15) gives expressions for the velocities in terms of A and C . Equation (21) gives z in terms of A and C , and also yields $A_1 = -A_2, C_1 = C_2$. Substituting the expressions for u and ζ in (24) and using (18) to define p , A and C can be eliminated to provide the dispersion relation, which is

$$(M + \nu_M) 2k^2\sigma + \sigma^2 + 4k^4 M \nu_M + \omega^2 - 4k^3(\mu_2 m_2 + \mu_1 m_1) \frac{M}{(\rho_1 + \rho_2)} = 0, \quad (25)$$

where

$$M = \frac{\mu_2 - \mu_1}{\rho_2 - \rho_1}, \quad \nu_M = \frac{\mu_2 + \mu_1}{\rho_2 + \rho_1}$$

and ω is the inviscid frequency for wavenumber k , i.e.

$$\omega^2 = \frac{(\rho_2 - \rho_1)g + j_s B_n + \alpha k^2}{\rho_1 + \rho_2} k.$$

3. Theoretical dispersion plots

3.1. Inviscid

To obtain meaningful information from the dispersion relation (11) above, which can assist in the planning of experiments to observe anisotropic waves, it is most useful to consider ω as given, and for simplicity to take the case of j and B imposed mutually at right angles so that $j_s B_n$ is $JB \cos^2 \theta$, θ being the angle between \mathbf{B} and \mathbf{n} , and J is the imposed current density, positive for $\mathbf{j}_s \times \mathbf{B}_n$ acting downwards and negative when $\mathbf{j}_s \times \mathbf{B}_n$ acts upwards. Then phase and group velocity can be plotted in polar form as functions of θ , for a given ω , having eliminated k .

We shall consider only waves in a deep fluid, such that h_1 and h_2 are greater than half a wavelength and $\coth kh = 1$ is a reasonable approximation. The results for long waves in shallow fluids are similar (Robinson 1973). Then the phase velocity ($c = \omega/k$) is

$$c^3 - \frac{(\rho_2 - \rho_1)g + JB \cos^2 \theta}{(\rho_1 + \rho_2)\omega} c^2 - \frac{\alpha\omega}{\rho_1 + \rho_2} = 0, \quad (26)$$

and \mathbf{c} is in the \mathbf{n} direction.

The group velocity has two polar components, $C_k = (\partial\omega/\partial k)_\theta$ in the \mathbf{n} direction, and $C_\theta = k^{-1}(\partial\omega/\partial\theta)_k$ in the \mathbf{s} direction. Hence

$$C_k = \frac{(\rho_2 - \rho_1)g + JB \cos^2 \theta}{2\omega(\rho_1 + \rho_2)} + \frac{3\alpha\omega}{2c^2(\rho_1 + \rho_2)}, \quad (27)$$

$$C_\theta = -\frac{JB \sin 2\theta}{2\omega(\rho_1 + \rho_2)}. \quad (28)$$

Equations (26)–(28) must be solved on a computer for a range of θ and ω for given physical parameters, since it is not possible to rationalize the equations with surface tension into a form dependent only upon one dimensionless parameter, as Shercliff does using $\gamma = JB/(\rho g)$. Moreover, the form of the dispersion relation (11) is such that the polar plot of the group velocity vector is not the same shape as a line of constant phase, as it is when surface tension is neglected. The line of constant phase is a useful concept for experimental wave observation,

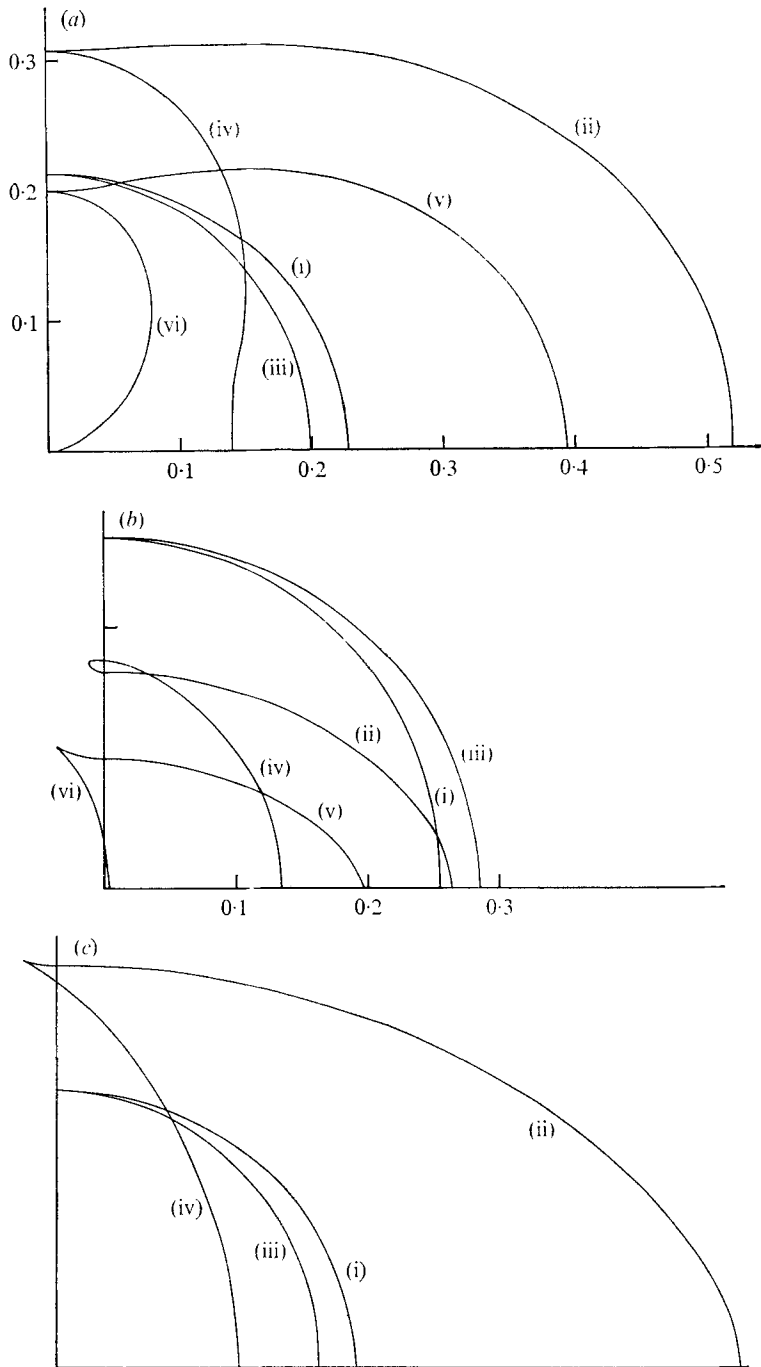
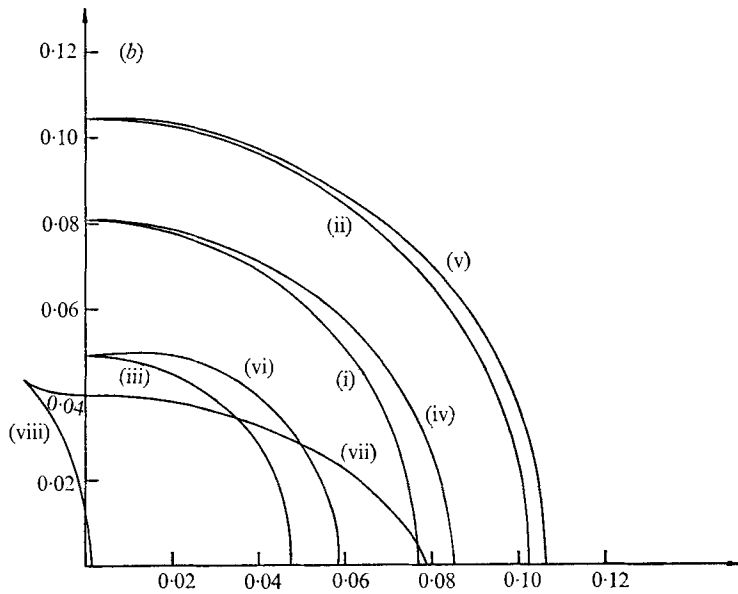
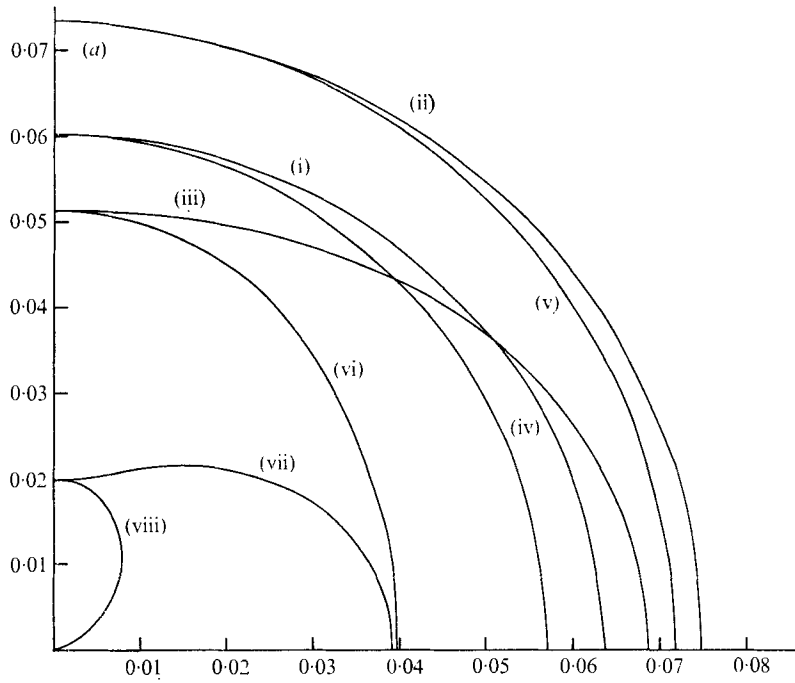


FIGURE 2. Polar dispersion plots: surface waves on mercury. \mathbf{B} is parallel to the x axis. Specific gravity 13.6. Surface tension 0.5 N m^{-1} , $B = 0.2 \text{ Wb m}^{-2}$, $J = 5 \times 10^5 \text{ A m}^{-2}$. (a) Phase velocity (m s^{-1}). (b) Group velocity (m s^{-1}). (c) Lines of constant phase.

Force	Down		Up			Down	Up
Frequency (rad s^{-1})	(i)	(ii)	(iii)	(iv)	Zero surface tension } (not to scale)	(v)	(vi)
	200	33	200	33			



FIGURES 3(a, b). For legend see next page.

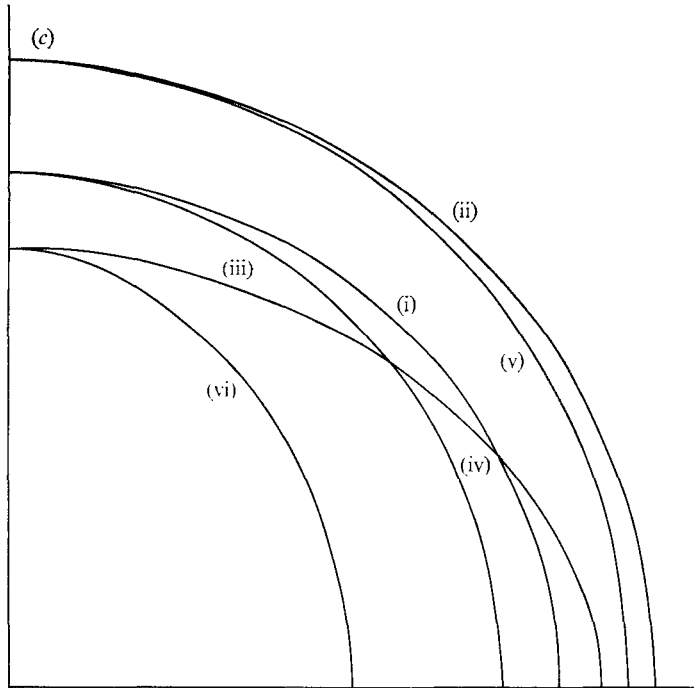
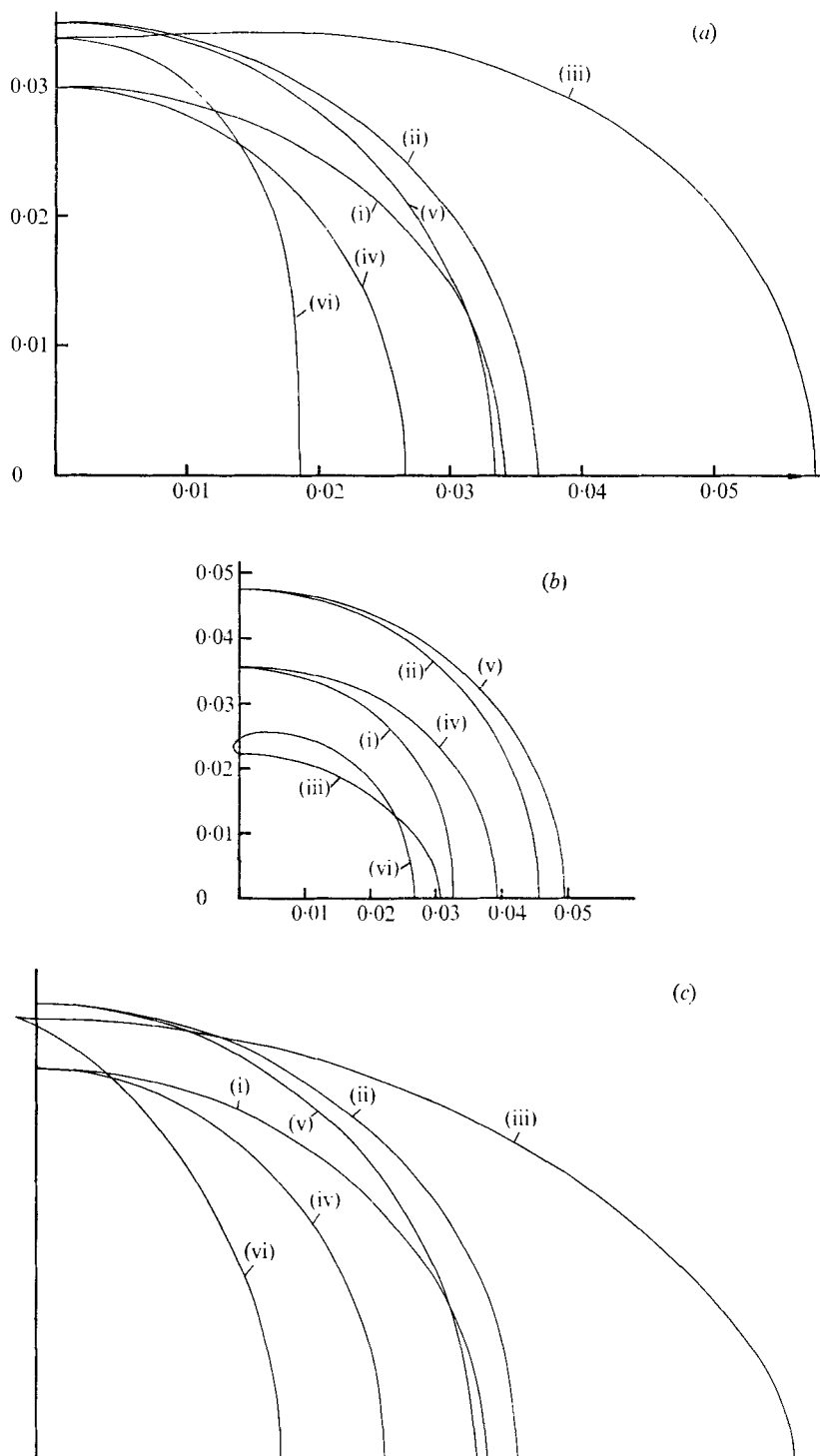


FIGURE 3. Polar dispersion plots: interfacial waves between electrolyte and an organic solvent mixture. \mathbf{B} is parallel to the x axis. Specific gravity: upper fluid, 1.080; lower, 1.101. Interfacial tension 0.04 N m^{-1} . $B = 0.2 \text{ Wb m}^{-2}$, $J = 10 \text{ A m}^{-2}$. (a) Phase velocity (m s^{-1}). (b) Group velocity (m s^{-1}). (c) Lines of constant phase.

Force	Down			Up			Down	Up
Frequency (rad s^{-1})	(i) 10	(ii) 20	(iii) 3.33	(iv) 10	(v) 20	(vi) 3.33	Zero surface tension } (vii)	(viii)
							(not to scale)	

since it represents the shape of wave crests and troughs which will occur owing to a point wave source of constant frequency in a surface of infinite extent, provided crests are considered far enough away from the source for the plane wave assumption to be valid (i.e. the wavelength is small compared with the distance from the source). The shape of lines of constant phase can be obtained as the envelope of normals to the extremity of the phase velocity vector \mathbf{c} , but, to facilitate the programming of a computer to plot such lines, use is made of the fact that such normals touch the envelope at a point whose direction from the origin is that of the group velocity corresponding to \mathbf{c} (Shercliff 1970).

Polar plots of \mathbf{c} , \mathbf{C} and lines of constant phase are drawn in figures 2-4 for values of θ from 0 to $\frac{1}{2}\pi$. The full $0 \rightarrow 2\pi$ plots can be obtained by reflexion in both axes. The physical parameters indicated in the captions were chosen as representative of typical possible experimental conditions, to be discussed in §4. Figure 2 is for waves on the surface of mercury; and figures 3 and 4 represent waves at the interface of two fluids closely matched in density, with and without the addition of a surface-tension reducing agent. Only one value of the ratio $JB/[(\rho_2 - \rho_1)g]$ is used, the maximum which can practically be

FIGURE 4. As for figure 3, but at surface tension 0.004 N m^{-1} .

obtained, representing the greatest degree of anisotropy which could be obtained. Both upward and downward acting $\mathbf{j} \times \mathbf{B}$ forces (i.e. positive and negative J) are considered.

When comparison is made with Shercliff's theoretical plots, the influence of surface tension is apparent. Not only is the anisotropy reduced by surface tension, but also it becomes frequency dependent, and the plots tend to circles as the frequency increases. Moreover, the difference between the group-velocity plot and the lines of constant phase is obvious, the latter being the same cusped shape in extreme cases as for zero surface tension, but with the group-velocity locus looped instead of cusped. Ideally, a laboratory experiment would aim to produce these cusped lines of constant phase, since they present the most interesting case to study; but the inclusion of surface tension in the analysis demonstrates that the practical problem is more complex than simply providing a large enough $\mathbf{j} \times \mathbf{B}$ force to compete with gravity, as might have appeared at first sight. The influence of surface tension diminishes with decreasing frequency; but this involves catering for larger wavelengths, and hence a larger scale of experiment, which is much harder to achieve in an MHD situation than the OHD case, because of the need to provide a magnetic field and electric current supply over a correspondingly larger working volume. It is useful to have an indication of the dependence of anisotropy upon frequency; this is shown in figure 5, a plot of the anisotropy ratio $R(\omega)$ against frequency, where

$$R(\omega) = c_{\theta=0}/c_{\theta=\frac{1}{2}\pi}.$$

($c_{\theta=0}$ is the phase velocity for maximum MHD effect, and $c_{\theta=\frac{1}{2}\pi}$ is the OHD case.) Figure 5 is drawn for the two-fluid case of figures 3 and 4, with an additional, intermediate surface-tension value. It records that, against expectation created by the theory ignoring surface tension, the degree of anisotropy obtainable with a downward $\mathbf{j} \times \mathbf{B}$ force is comparable with that for an upward force of the same magnitude, since the latter case, having reduced wavelengths, is more influenced by surface tension. Thus, because there is no stability limit on the downward force, it may be possible to achieve the greatest anisotropy by this means. Figure 6 shows frequency against wavenumber for the same parameters.

3.2. *Viscous dispersion relation*

The viscous dispersion relation (25), after substitution for m_1 and m_2 , becomes a polynomial of order 8 in σ , k or c , whichever is chosen as the dependent variable. As such, it is not strictly a wave equation, but the solutions will approximate to waves if the coefficients of even-order terms in σ are very much greater than odd-order ones. If this is so, we would expect damped oscillations, and an estimate of the damping can be obtained if we let $\mu_1 = \mu_2$, whence $M = 0$, and (25) becomes

$$\sigma^2 + \omega^2 + 2\nu_M k^2 \sigma = 0, \tag{29}$$

having the solution $\sigma = i\omega - k^2\nu_M$ provided $\omega^2 \gg k^4\nu_M^2$. Now ω is the term containing the anisotropy; so, provided this condition holds, the anisotropy is the same in the viscous case as the inviscid. But, with an upward $\mathbf{j} \times \mathbf{B}$, k is

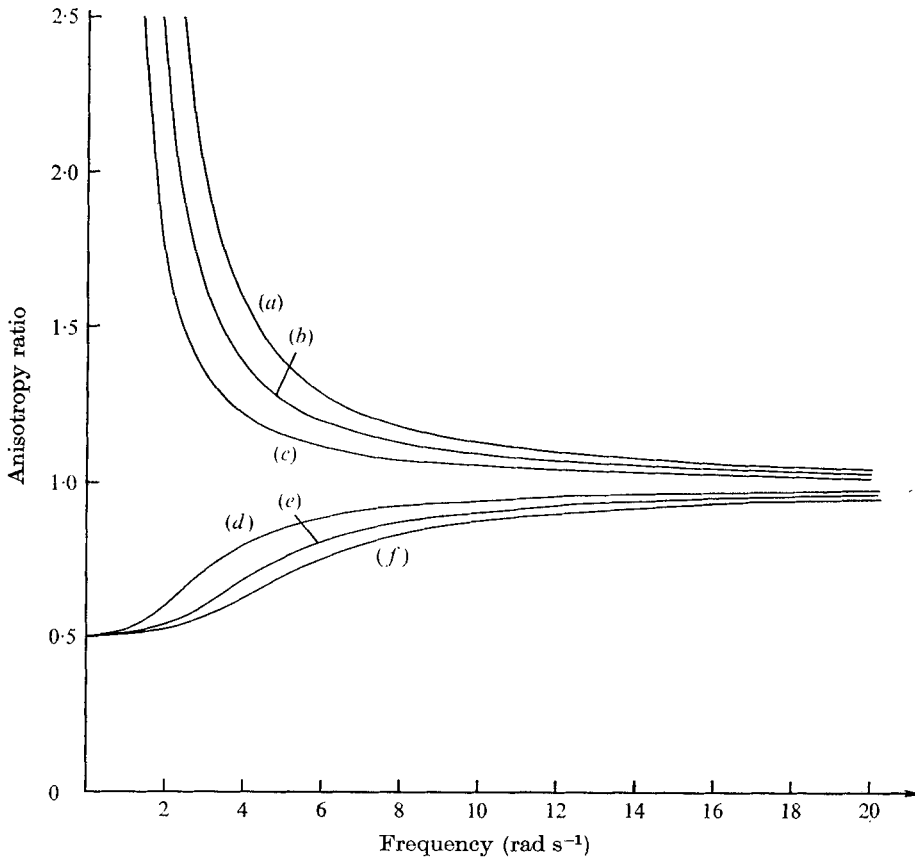


FIGURE 5. Anisotropy ratio against frequency.

Force	Up			Down		
α (N m^{-1})	(a)	(b)	(c)	(d)	(e)	(f)
	0.004	0.010	0.04	0.004	0.010	0.04

increased in one direction; so damping is increased, and it is harder to meet the condition on ω . It is necessary to consider (25) separately for each set of parameters, to see the effect of viscosity for particular cases.

4. Choice of experimental parameters

4.1. *The choice of working fluids*

In any MHD experiment, while flexibility is gained from the larger range of parameters which influence the process under consideration, the choice of working fluids and materials for the containing vessel and ancillary equipment is often severely limited by the requirement that such materials have a suitable combination of fluid mechanical and electromagnetic properties. In planning an experiment to observe MHD anisotropic surface waves, three different systems present themselves as possibilities: (i) the use of a sodium-potassium

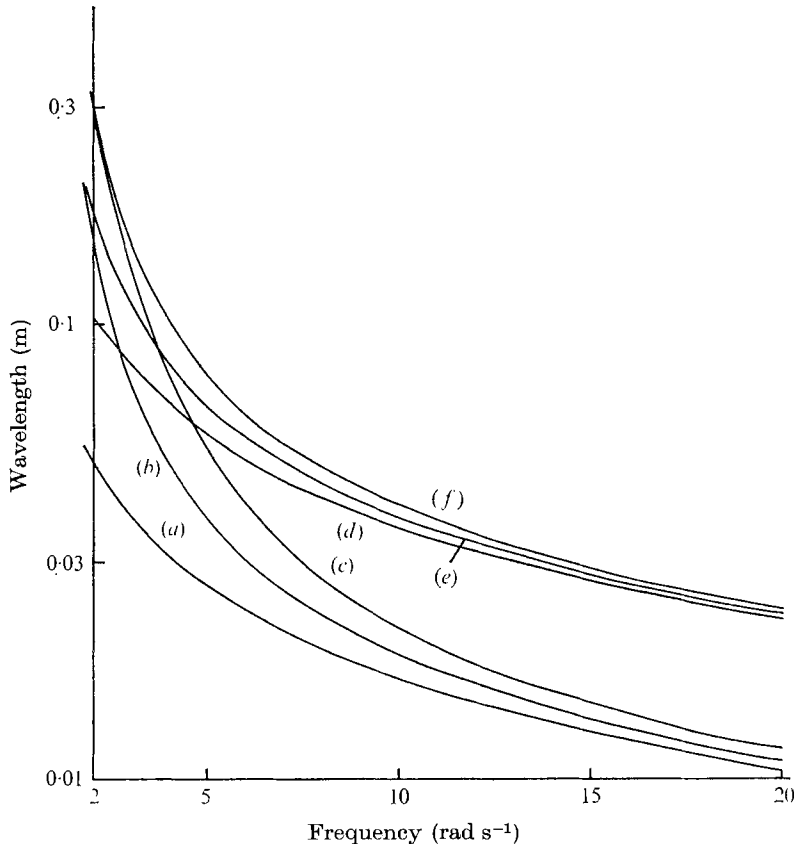


FIGURE 6. Wavelength against frequency. Force: (a), (d) up, wave normal in \mathbf{B} direction; (b), (e) none, or wave normal in \mathbf{J} direction (OHD wave); (c), (f) down, wave normal in \mathbf{B} direction. (a)–(c) $\alpha = 0.004 \text{ N m}^{-1}$; (d)–(f) $\alpha = 0.04 \text{ N m}^{-1}$.

eutectic mixture, of necessity covered by an organic liquid to prevent spontaneous ignition, waves being observed at the interface; (ii) surface waves on mercury; and (iii) an electrolytic conducting liquid, which can only pass relatively low currents compared with the liquid metals, and thus needs to be covered by an immiscible liquid of similar density, if MHD forces are to be able to compete with gravity forces to influence interfacial waves.

The experiments to be described used (iii). (i) was eliminated because of the complexities of handling liquid sodium in safety. Use of mercury (suggested by Shercliff) was tried; but, with a direct current source limited to 1000 A in our laboratory circumstances, and a required current density of $5 \times 10^5 \text{ A m}^{-2}$, the maximum surface width was 70 mm, insufficient for the propagation of surface waves unaffected by reflexions from the wall. Moreover, it would be difficult to observe the wave patterns on a large surface area of mercury, by reflective methods.

Having decided on a basic system, the choice of working fluids was still difficult, in that both fluids had to satisfy conditions of low viscosity (i.e. of the

order of the viscosity of water); be transparent to light to allow visual observation, and of significantly different refractive index to reveal interfacial waves by a shadow technique; have as low an interfacial tension as possible; be immiscible and insoluble in each other; and be of similar density. The electrolyte had to be chosen with as good a conductivity as possible, and minimal polarization and generation of by-products at the electrodes. Both liquids needed to be safe to handle, as regards both toxicity and flammability, readily available and relatively cheap.

The obvious choice of electrolyte was copper sulphate solution in conjunction with copper electrodes. Although not as good a conductor as HCl, it is less corrosive, presents less electrode problems, and a solution with specific gravity of 1.10 was found to be capable of carrying a current density of 1000 A m^{-2} under an electric field of about 300 V m^{-1} . A suitable upper, non-conducting fluid was harder to find; but finally a mixture of white spirit (turpentine substitute) with S.G. of 0.85 and Genklene (1,1,1-trichloroethane) with S.G. 1.32 was used. By mixing these in suitable proportions, the specific gravity could be varied to match that of the electrolyte. The interfacial tension between the electrolyte and the organic solution was estimated to be 0.04 N m^{-1} , from observing the meniscus rise in a small length of capillary tube with one end in each fluid, assuming zero angle of contact. By adding about 5 cm^3 Teepol to 10 litres of electrolyte, the interfacial tension could be reduced to 0.004 N m^{-1} . The two fluids were not noticeably miscible at room temperatures; but, with the addition of Teepol, and after the copper sulphate had been heated ohmically, the interface became blurred by contamination of one fluid by the other and by products of electrolysis, restricting the useful life of a batch of fluid to two or three runs of half an hour each.

4.2. *The scale of the experiment*

To be able to make worthwhile observations of waves without the interference of reflexion at the walls of the vessel, the length scale of the tank must be an order of magnitude greater than the anticipated wavelength, in both horizontal directions, to provide scope for waves of any orientation. The depth of each fluid must be at least half the anticipated wavelength. But a magnetic field of 0.2 Wb m^{-2} must be supplied over the whole area, as uniformly as possible; and a total current, proportional to the length times the depth, must be supplied at a voltage proportional to the length scales; this requires the use of as small a scale as possible. At the same time, one must overcome surface-tension effects by using as large a scale as possible. Figure 5 is of use in making the necessary compromise, showing that to obtain a degree of anisotropy which will show up convincingly in an experiment, a frequency of less than 10 rad s^{-1} must be used, preferably less than $2\pi \text{ rad s}^{-1}$. From figure 6 it may be seen that 10 rad s^{-1} corresponds to wavelengths of 12–40 mm, wavelengths being at lower frequencies. Hence, it was decided that the wave tank should be at least 500 mm square, and of sufficient depth to take at least 25 mm depth of each fluid, catering for maximum wavelengths of about 50 mm.

ρ_1				1.080×10^3	
ρ_2				1.100×10^3	
B				0.2	
j				1000	
μ_2				1.0×10^{-3}	
μ_1				1.3×10^{-3}	
ν_2				0.9×10^{-6}	
ν_1				1.2×10^{-6}	
α		0.004			0.04
ω (rad s ⁻¹)		1.5 × 2π		1.0 × 2π	
k (rad m ⁻¹)		43 × 2π	58 × 2π	16 × 2π	21 × 2π
$(M + \nu_M) 2k^3\sigma$		2.4 σ	4.25 σ	0.32 σ	0.56 σ (a)
σ^2		σ ²	σ ²	σ ²	σ ² (b)
$4k^4 M \nu_M$		0.33	1.07	6.33×10^{-3}	19.6×10^{-3} (c)
ω^2		90	90	40	40 (d)
$\frac{4k^3 M(\mu_2 m_2 + \mu_1 m_1)}{(\rho_1 + \rho_2)}$		$1.25 \sigma^{\frac{1}{2}}$	$3.1 \sigma^{\frac{1}{2}}$	$0.063 \sigma^{\frac{1}{2}}$	$0.15 \sigma^{\frac{1}{2}}$ (e)

TABLE 1. Relative magnitude of terms in the dispersion equation (25) involving viscosity (all in SI units).

4.3. The validity of the theoretical approximations

Shercliff (1969) discussed the conditions necessary for the electromagnetic approximations and assumptions to be valid. It is necessary to show that the experimental parameters used here satisfy the necessary small-value criteria.

We take B as 0.2 Wb m^{-2} , being a value that can reasonably be obtained in the laboratory, but which is not so high as to make ohmic damping a problem with copper sulphate solution (the conductivity of which was measured to be around 4 mho m^{-1}). Given $(\rho_2 - \rho_1) \approx 20 \text{ kg m}^{-3}$, $J \approx 10^3 \text{ A m}^{-2}$. The depth of the conducting fluid is typically 30 mm ; typical values for ω and k are 10 rad s^{-1} and 100 rad m^{-1} , respectively. Taking the magnetic permeability $\mu = 1.2 \times 10^{-6}$, $g = 10 \text{ m s}^{-2}$, the ratios that must be small are

$$\text{small effect of } j \text{ on } B \quad \mu J h / B = 1.8 \times 10^{-4},$$

$$\text{small damping by induced } j \quad \sigma B^2 / \rho \omega = 1.6 \times 10^{-5},$$

$$\text{small } \nabla \times \mathbf{E} \quad \mu \sigma \omega / k^2 = 4.8 \times 10^{-9}.$$

Clearly the use of an electrolytic rather than a metallic conductor makes the electromagnetic assumptions even more realistic.

It remains to consider the effect of viscosity, by inspecting the relative magnitude of the terms in (25) with the inviscid estimates of ω and k inserted. Taking two different surface tension and frequency combinations, corresponding to the maximum inviscid frequency to produce reasonable anisotropy at the given surface tension, the approximate values of individual terms expressed as multiples of powers of σ are given in table 1. For each ω , there are two values of k , representing the least and greatest wavenumbers occurring in the inviscid anisotropic situation. If it is assumed that $\sigma \approx \omega$, then, for the given parameters,

$m \approx (\sigma/\nu)^{\frac{1}{2}}$, and hence term (e) can be evaluated as a multiple of $\sigma^{\frac{1}{2}}$. If the assumption $\sigma \approx \omega$ is valid (i.e. viscosity does not significantly alter the predicted inviscid wave pattern), then (b) and (d) must be an order of magnitude greater than the other terms. When we substitute $\sigma = \omega$, this is seen to be so for higher surface tension with lower frequency. However, for the shorter wavelength at the lower surface tension, (a) and (e) approach $\frac{1}{3}$ of (d), showing that the inviscid approximation is being pushed to the limit by these parameters. Therefore any further steps to improve the possibilities of producing anisotropy (either by matching densities more closely or by further reduction of surface tension) would be futile, since viscosity would then tend to dominate the wave motion.

5. The experimental rig

To provide the necessary magnetic field, a Helmholtz coil pair was designed and built by the UKAEA Culham Laboratory. Based on a mean diameter of 1 m, the centres 0.5 m apart, the coils produced a field of 0.22 Wb m⁻² to within 5% over a central cubic volume of side 0.5 m, when drawing 1000 A d.c. at 60 V from a motor generator set. To reduce cost considerably, water-cooled aluminium hollow-section was used as the coil conductor, and proved as satisfactory as copper, except for the somewhat increased bulk. The use of Helmholtz coils, rather than an iron-cored magnet, left the working section open to view from all six sides, making observation of the waves easier. Further details of all the equipment are given by Robinson (1973).

The current supply to the copper sulphate was from the a.c. mains controlled by a 20 A auto-transformer and full wave rectified through a diode bridge. No attempt was made to smooth the ripple on the resulting d.c., since the 100 Hz frequency is not 'felt' by the fluid. Rather than using copper sheet, the electrodes were constructed of copper gauze, mesh size 28 per inch, because it proved less prone to serious contamination by products of electrolysis. This is important, because any variation in contact resistance across the electrode face produces a non-uniform current density field in the fluid which results in rotational $\mathbf{j} \times \mathbf{B}$ forces and hence the generation of fluid motion.

The fluids were contained in a Perspex tank, 0.6 m square, with a Perspex lid floating on the upper liquid to reduce evaporation and consequent density variations, as well as to eliminate surface waves. Figure 7 is a diagram of the apparatus. Beaches with a 10° slope were provided at the level of the interface, to hinder the reflexion of interfacial waves, but this was found to be unnecessary, because the waves were considerably damped by viscosity by the time they reached the walls. The false floor deepened into trenches to take the electrodes, providing a larger surface area of electrode to cope with the current. This was possible because the tank was being used only for \mathbf{j} perpendicular to \mathbf{B} ; otherwise, such an arrangement would result in rotational $\mathbf{j} \times \mathbf{B}$ forces. To ensure good electrode contact, the copper sulphate was fed into the tank first, by a tube through the wall into the electrode trough, before the organic liquid was bubbled slowly into place above it.

The wavemaker was a push rod and cam assembly, driving a thin Perspex

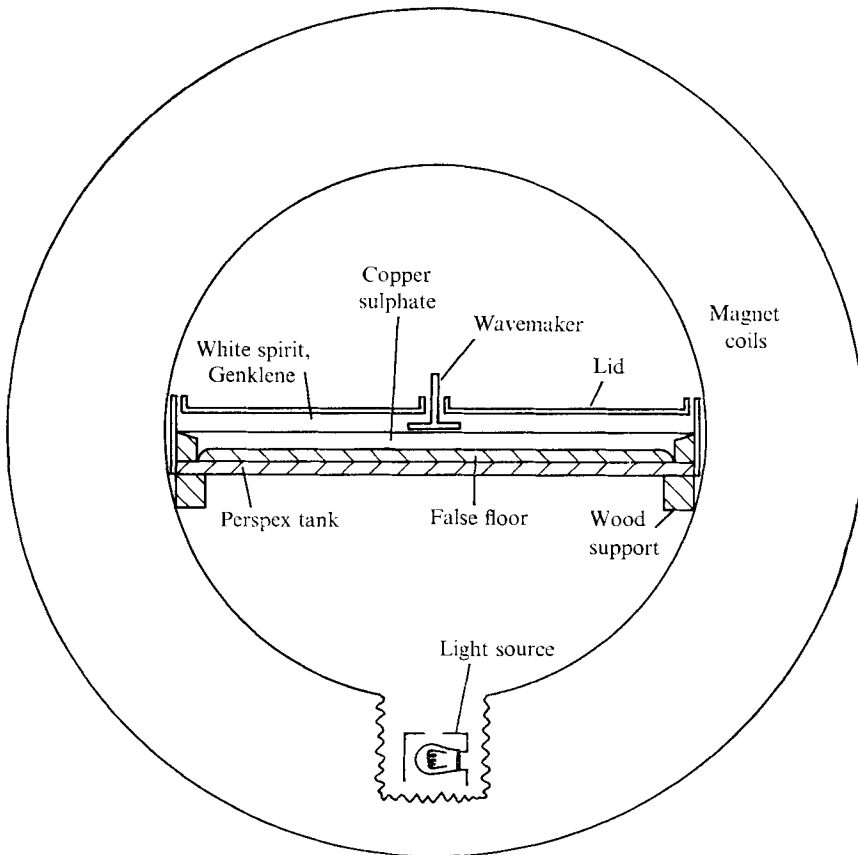


FIGURE 7. Diagram of apparatus.

sheet, round for a point wave source and rectangular for a line wave source, parallel to the plane of the interface but wholly in the upper fluid. Although energy transfer to the waves was reduced thereby, this arrangement was necessary to prevent any mean distortion of the interface by capillary effects, which had been found to distort the current flow pattern sufficiently to produce spurious fluid motion through rotational $\mathbf{j} \times \mathbf{B}$ forces. Since such spurious motion leads to distortion of the wave patterns, its elimination is vital; but, without using a two-fluid system, there is no obvious way of completely eradicating it.

The waves were observed by illuminating the tank by a bright point source of light 0.5 m below it, and casting the pattern resulting from the refraction at the interface upon a sheet of tracing paper laid on the lid. The distance between the interface and the lid being only about 35 mm, the patterns of dark and light on the paper bore a direct relation to troughs and crests of interfacial waves. Records of wave patterns were made by photographing the images on the tracing paper. Because of their green-blue colour, it was found necessary, if good contrast was to be obtained on the negatives, to use a double orange filter with a 400 ASA panchromatic film, force developed. Contrast was assisted by enclosing the whole apparatus in a blackout tent.

6. Observations of wave anisotropy

To demonstrate the anisotropy of the phase velocity, plane waves were generated by a wavemaker consisting of a 40×400 mm sheet of 1.5 mm thick Perspex, braced for rigidity by a thicker bar of Perspex fixed to the centre of the upper side. The wavemaker could be rotated to any orientation, so that the angle θ between wave normals and the magnetic field direction could be varied between 0 and 90° , to enable comparison with the theoretical curves of figures 3 and 4.

There are considerable problems in a direct comparison of observed and theoretical phase velocities, in that it is difficult to measure the physical parameters accurately. Specific gravity of the upper and lower fluids can be measured by hydrometer before the experiment to the nearest 0.001, which is about 5% of the difference between them; but heating during the experiment and the possibility of differential evaporation of the upper fluid mixture introduce unknown density variations during an actual run. Similarly, not only is it difficult to measure accurately the interfacial tension beforehand, but this also can vary considerably during a run, owing to contamination of the interface. Nonetheless, it is possible to make reasonable estimates of the physical parameters, by using the pre-run values and calculating surface tension from a knowledge of frequency and wavelength in the OHD case. To avoid any doubt in the area of whether or not anisotropy exists, the following experimental procedure was adopted.

A run consisted of filling the tank with newly prepared fluids of measured densities, setting the wavemaker at a fixed frequency, which was checked by stop watch at intervals during the run, and then, with the wavemaker at each of a series of orientations, taking two photographs of the wave pattern, before and after the current was switched on to a set value. The magnetic field was kept on all the time. By this procedure, even if the parameters varied significantly throughout the run, there should have been negligible variation between the consecutive photographs without and with the current on at the same orientation. Thus, any variation in wavelength between such photographs is evidence of the effect of the $\mathbf{j} \times \mathbf{B}$ force only. Typical pairs of photographs are shown in figure 8 (plates 1 and 2). The waves show up as light and dark bands parallel to the wavemaker, which is visible at the bottom of the field of view. Wavelength ratios were measured from the photograph pairs, and polar plots were made of the ratio against different orientations of the wave normal. Since the wavelength without current on should be the same for any orientation, if the physical parameters remain constant, plotting the ratio instead of the actual MHD wavelength effectively normalizes the results to eliminate the influence of varying density and surface tension. The results are compared with the theoretical plot, corresponding to the initial values of density and the mean of surface-tension values calculated from each OHD photograph. Figure 9 shows the results from typical runs at three different frequencies, with theoretical curves constructed for comparison. Clearly, the observed waves were anisotropic in such a way as to give a general agreement with the theoretical curves. Figure

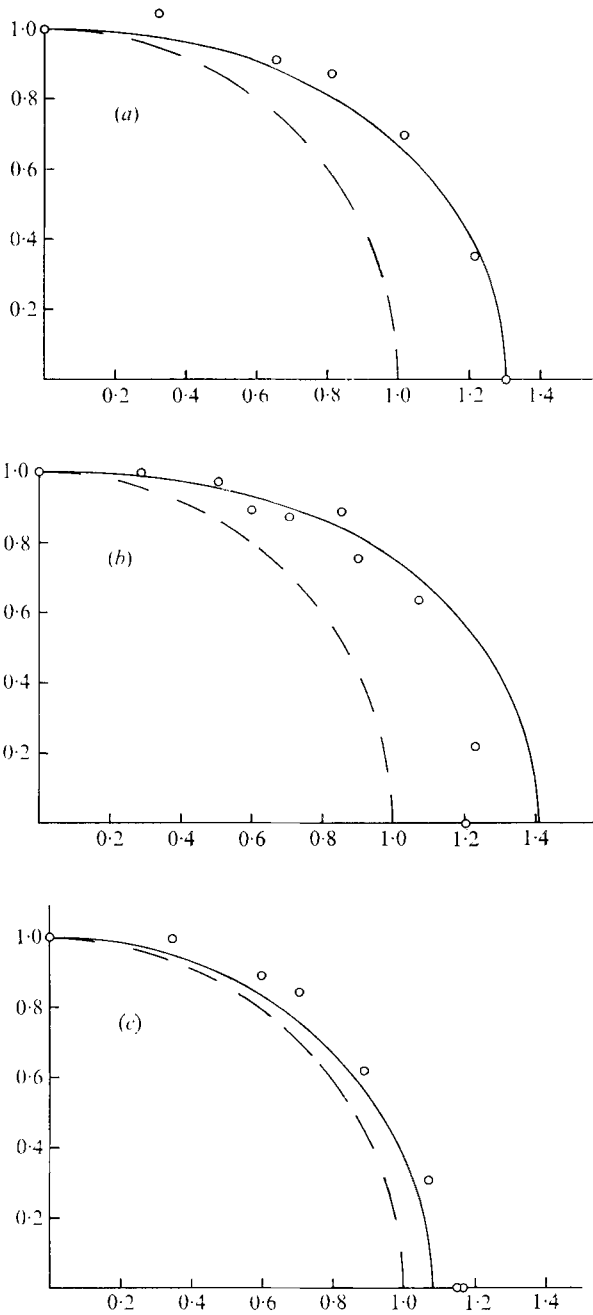


FIGURE 9. Polar graphs of wavelength ratio against θ . The \mathbf{B} is parallel to the x axis.
 $\rho_1 = 1071 \text{ kg m}^{-3}$, $\rho_2 = 1094 \text{ kg m}^{-3}$, $B = 0.192 \text{ Wb m}^{-2}$, $J = 850 \text{ A m}^{-2}$.

	ω (rad s ⁻¹)	Estimated surface tension (N m ⁻¹)
(a)	3.74	0.018
(b)	3.98	0.006
(c)	8.85	0.019

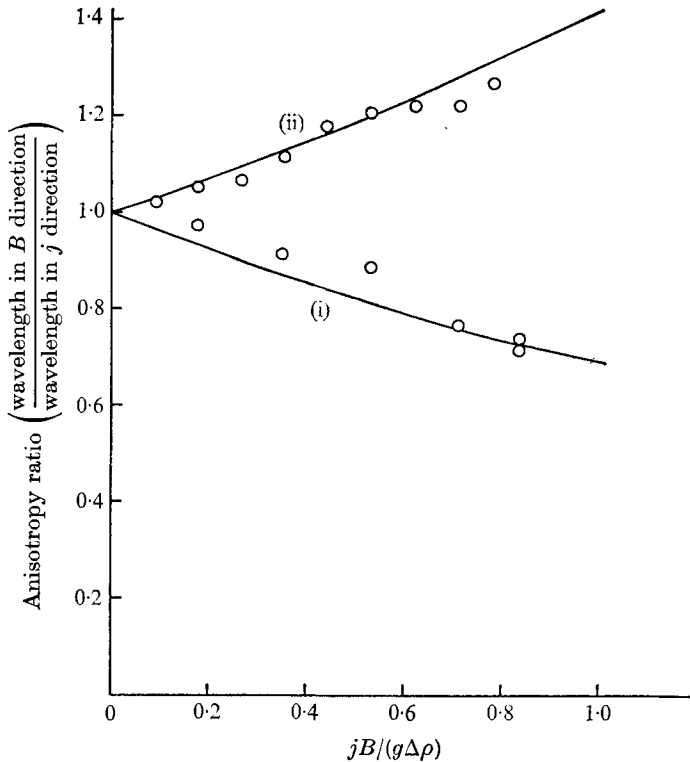


FIGURE 10. Anisotropy ratio against $\mathbf{j} \times \mathbf{B}$ force. $\rho_1 = 1071 \text{ kg m}^{-3}$, $\rho_2 = 1094 \text{ kg m}^{-3}$, $B = 0.192 \text{ Wb m}^{-2}$. (i) Upward force, $\omega = 3.45 \text{ rad s}^{-1}$, $\alpha = 0.019 \text{ N m}^{-1}$. (ii) Downward, $\omega = 3.98 \text{ rad s}^{-1}$, $\alpha = 0.018 \text{ N m}^{-1}$.

9(a) represents the closest agreement between theoretical and experimental results, while, for the other two cases, the experimental results are closer to the theoretical curve than to the isotropic (dotted curve). Considering the difficulty of estimating parameter values, as mentioned above, and the error (probably $\pm 5\%$) in measuring wavelength ratios from the photographs, it is considered that the results of this experiment support the theoretical predictions within the rather wide limits of accuracy of the apparatus. At the least, the existence of anisotropic surface waves has been verified.

Further runs were performed for waves having normals in the \mathbf{B} direction, varying the current density and making comparison with the unaffected wave in the \mathbf{j} direction at the same frequency, surface tension and $jB/(\Delta\rho g)$ value. In figure 10 the ratio of wavelengths is plotted against the parameter $jB/(\Delta\rho g)$ for both upward and downward acting $\mathbf{j} \times \mathbf{B}$ forces, and compared with theoretical curves. Once again, a general agreement between experimental and theoretical values is observed, the scatter of the points and lack of close agreement being attributable to the measurement errors noted above.

Attempts were made to produce anisotropic lines of constant phase using a point wave source. But the reduction in wave amplitude as waves radiated from

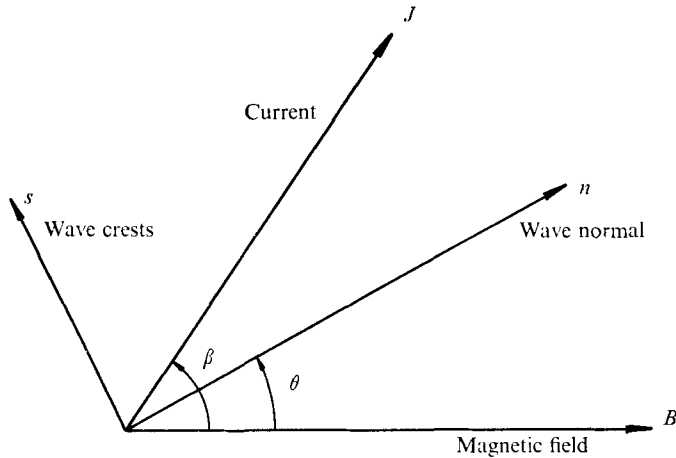


FIGURE 11

the source meant that only the shorter wavelength, higher frequency waves would show up clearly in the shadow technique. At these frequencies anisotropy was observed, but only to a very small degree (i.e. wavelength ratio > 0.95).

7. The dependence of the axis of anisotropy upon the relative orientations of \mathbf{j} and \mathbf{B}

The theory of MHD anisotropic surface waves predicts that the orientation of the axis of anisotropy varies as the angle between the imposed current and magnetic field is varied. This invites experimental verification. Rather than producing a polar plot of the phase velocity vector for each different angle between the imposed \mathbf{j} and \mathbf{B} , the basic theory can be tested by finding the orientation of the minimum phase velocity for a given \mathbf{j} and \mathbf{B} (i.e. the direction of the minor axis of the phase velocity quasi-ellipse). In practice, with an upward acting $\mathbf{j} \times \mathbf{B}$ force of sufficient magnitude, the phase velocity can be reduced to zero. Beyond this, increase of $\mathbf{j} \times \mathbf{B}$ causes the interface to become unstable; and the mode of instability is clearly the same as the mode of minimum phase velocity when the interface is still stable, since the stability equation is identical with the dispersion relation. Hence, an experiment to observe the orientation of the instability modes may be used to supply information about the orientation of the anisotropy in the fully stable case.

If the angle between the imposed \mathbf{j} and \mathbf{B} is β , and that between the wave normal and \mathbf{B} is θ (as in figure 11), then $j_s B_n$ in (11) may be replaced by

$$j_s B_n = jB \sin(\beta - \theta) \cos \theta = \frac{1}{2} jB [\sin \beta + \sin(\beta - 2\theta)].$$

Now the minimum phase velocity (or alternatively the normal to the mode in which instability first occurs as the current is increased) is in a direction which makes $j_s B_n$ a minimum, i.e. for a given value of β

$$\sin(\beta - 2\theta) = -1, \quad \text{i.e.} \quad \theta = \frac{1}{2}(\beta + \frac{1}{2}\pi). \tag{30}$$

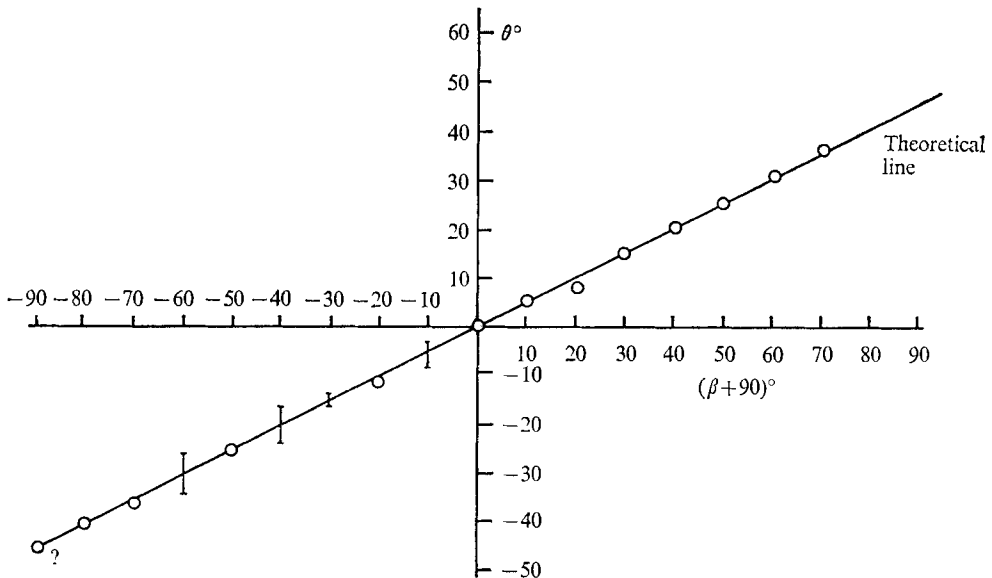


FIGURE 13. Results of orientation experiment.

Experimental verification. A tank was constructed to fit inside the magnet described above, the four corners resting on a circular brass track, enabling it to be rotated through 360° about a vertical axis through its centre. The sides of the tank were vertical, and the floor flat, so that there should be no rotational $\mathbf{j} \times \mathbf{B}$ forces produced by the geometry of the current flow when β is not 0° or $\pm 90^\circ$. As in the wave experiments, copper gauze electrodes were used, covering the whole wall on opposite sides of the tank. A system for photographic and direct visual observation of interfacial waves (and small-amplitude instabilities) was set up, as above. The tank rotated to set β at a given value; the magnetic field switched on; the imposed current was gradually increased until the surface began to become unstable. As predicted by theory, it did so in a wave form having parallel troughs and crests in one direction. When these had reached an amplitude of a few millimetres, sufficient to cast good shadows on the tracing paper of the lid, a photograph was taken (see figure 12, plate 3). As expected, as the tank was rotated progressively from a \mathbf{j} normal to \mathbf{B} position with $\mathbf{j} \times \mathbf{B}$ upward toward a \mathbf{j} and \mathbf{B} parallel or anti-parallel position, the current required to produce instability increased. The limits on available current prevented further rotation of the tank beyond the parallel position; but, even in this position, the required current was so high that spurious motions occurred, presumably due to rotational $\mathbf{j} \times \mathbf{B}$ forces, caused by very slight irregularities in the current distribution at the electrodes, magnified by the increased current.

From the photographs, θ was measured and plotted against β in figure 13. On one or two of the photographs, there was some ambiguity between two possible wave normals (as in figure 12(b)), and such results are shown as bars in figure 13. The theoretical line of (30) is drawn; and it can be seen that there is excellent agreement with experiment.

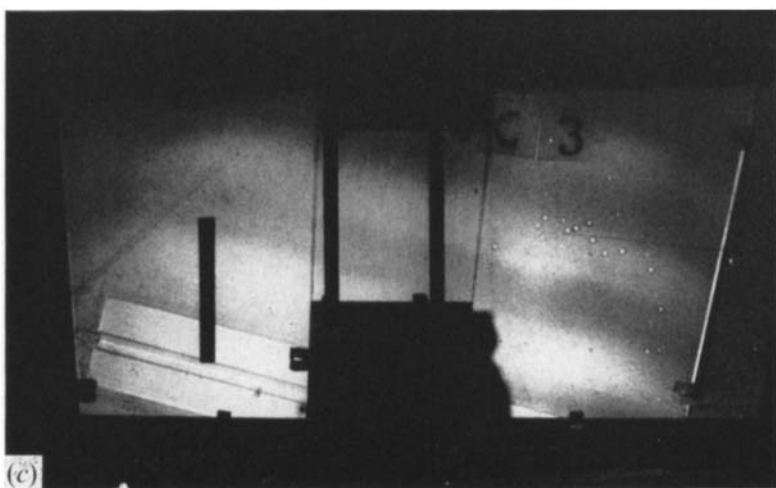
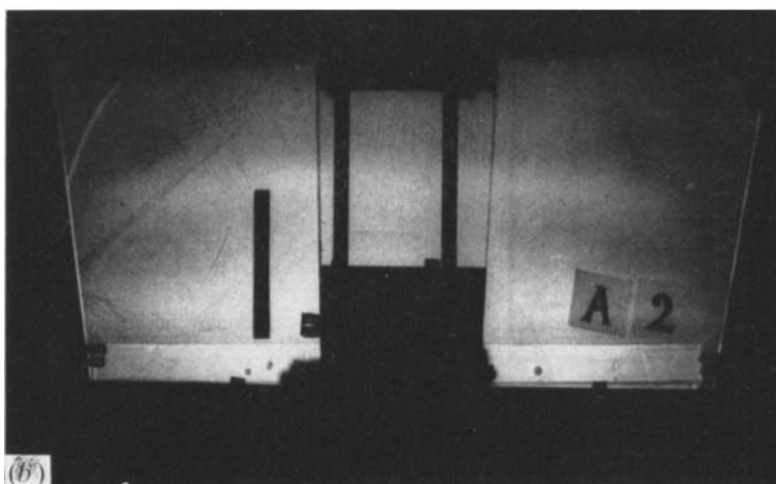
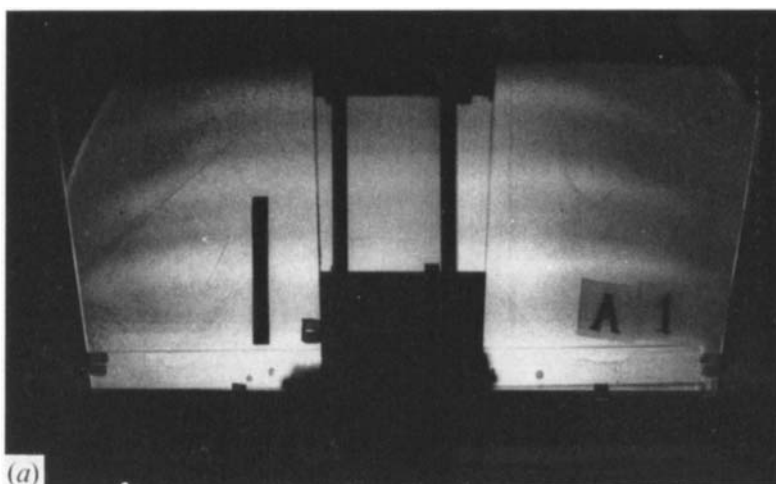
8. Conclusions

The existence of anisotropic surface waves due to a vertical electromagnetic body force was verified, and the analytical theory was substantiated within the rather wide limits of experimental accuracy. As it stands, the experiment does not provide an immediately convincing demonstration of anisotropic waves, since comparison must be made between consecutive runs. However, with further attention to the details of the experiment (e.g. increasing the amplitude of the wavemaker stroke and optimizing the size of the wavemaker), it should be possible to obtain more convincing anisotropic wave patterns from the point source experiment, which could then form the basis of a pedagogic technique for demonstrating anisotropic waves.

This work was carried out while the author received an SRC Studentship at the University of Warwick, Department of Engineering. The author thanks Professor J. A. Shercliff for the initial suggestion of the work and for helpful discussions throughout, and Mr A. E. Webb for assistance in the laboratory. He also acknowledges the support of the Institute of Oceanographic Sciences, Bidston, in the preparation of the paper.

REFERENCES

- BAKER, R. C. 1965 *Nature*, **207**, 65.
DUC, X. N. 1968 Etude théorique et expérimentale sur modèle hydraulique des instabilités de Rayleigh–Taylor en magneto hydrodynamique. *C.R. Acad. Sci. Paris, A* **266**, 738–740.
LAMB, H. 1932 *Hydrodynamics*. Cambridge University Press.
ROBINSON, I. S. 1973 Anisotropic surface waves and instabilities under a vertical electromagnetic force. Ph.D. thesis, University of Warwick.
SHERCLIFF, J. A. 1969 Anisotropic surface waves under a vertical magnetic force. *J. Fluid Mech.* **38**, 353.
SHERCLIFF, J. A. 1970 A note on the envelope construction for group velocity in dispersive anisotropic wave systems. *J. Inst. Math. Appl.* **6**, 91–95.



FIGURES 8 (a-c). For legend see plate 2.

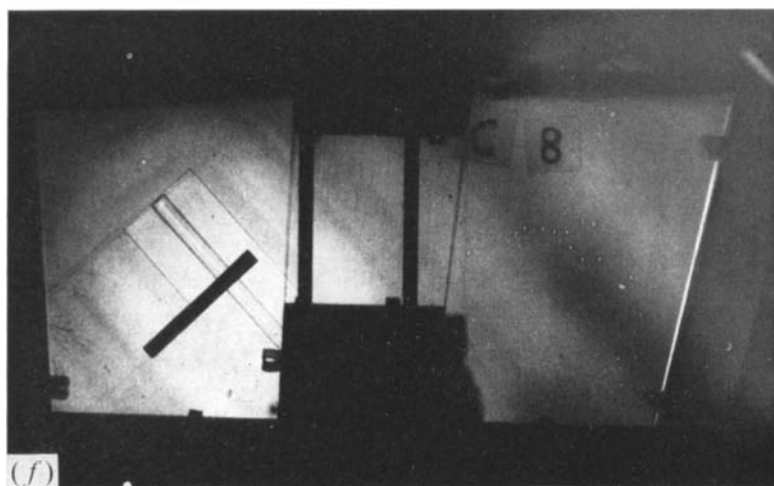
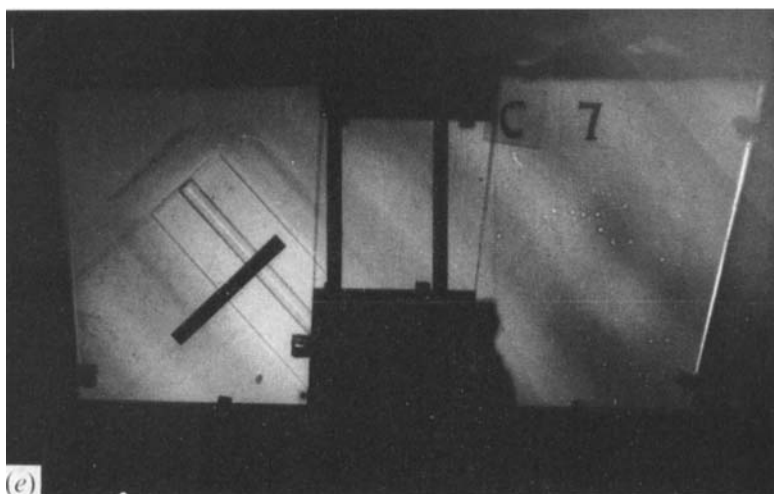
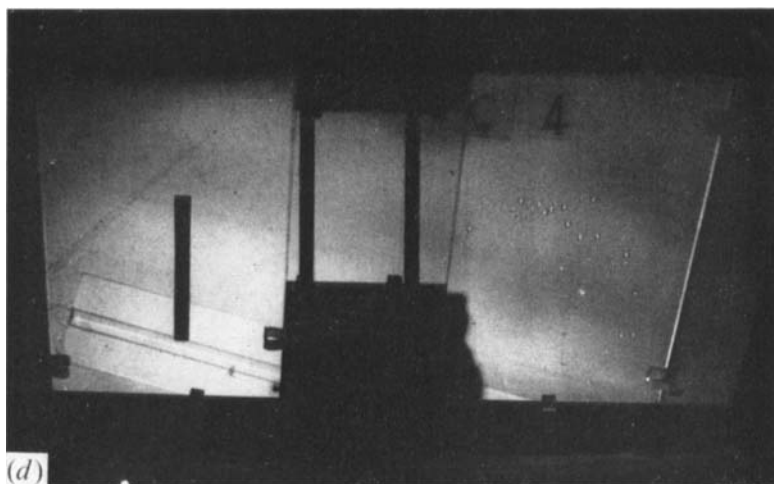


FIGURE 8. Typical photographs of plane waves.

	J ($A\ m^{-2}$)	B ($Wb\ m^{-2}$)	ω ($rad\ s^{-1}$)	α ($N\ m^{-1}$)	θ°	$\mathbf{j} \times \mathbf{B}$ force
Plate 1	(a) 0	0.192	3.98	0.006	0	Down
	(b) 920					
Plate 2	(c) 0	0.192	8.85	0.019	16	Down
	(d) 850					
Plate 2	(e) 0	0.192	9.85	0.019	47	Down
	(f) 850					

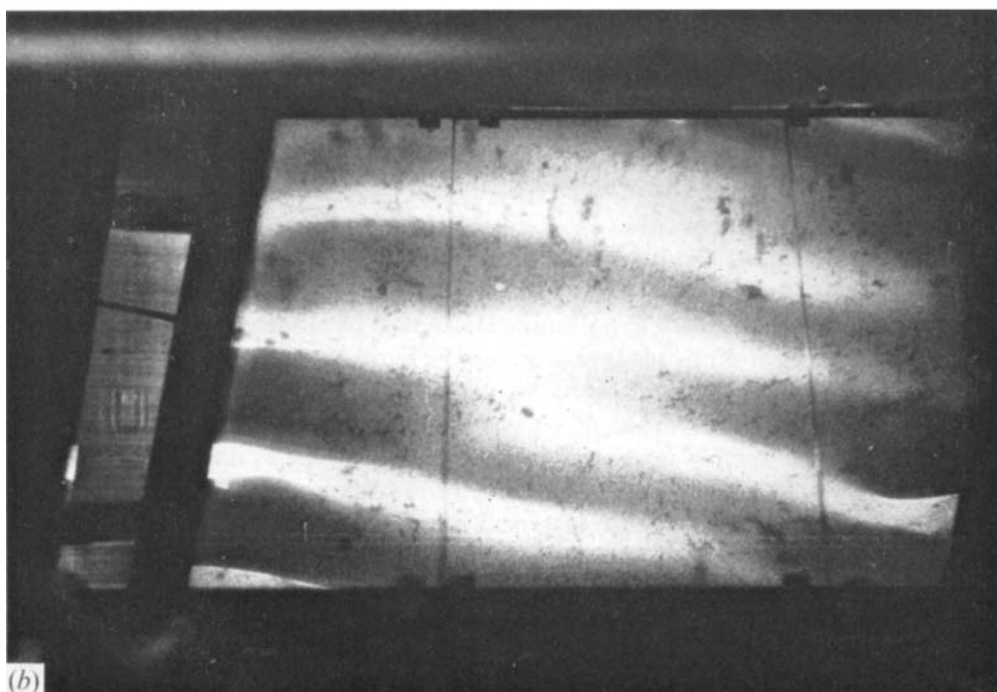
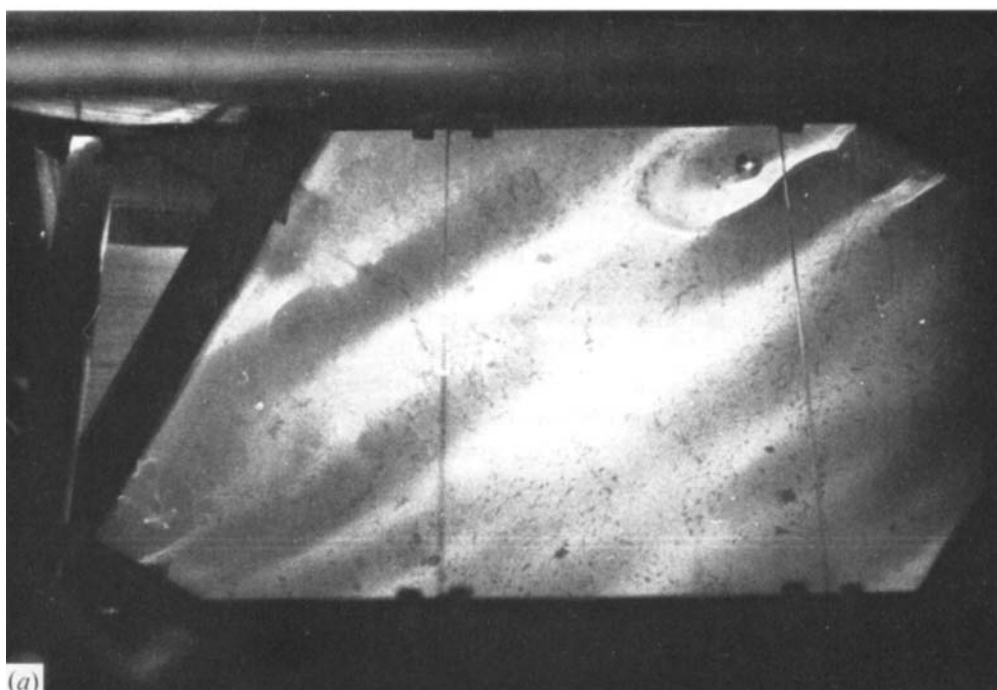


FIGURE 12. Typical photographs of instabilities in orientation experiments.

(a) $\beta = -30^\circ$. (b) $\beta = -100^\circ$.

ROBINSON